Supporting Information: Rigidifying of the internal dynamics of amyloid-beta fibrils generated in the presence of synaptic plasma vesicles.

Liliya Vugmeyster,[a*] Dan Fai Au,[a] Bailey Frazier,[a] Wei Qiang,[b] Dmitry Ostrovsky[c]

[a]*Department of Chemistry, University of Colorado Denver, Denver CO USA 80204*

[b]*Department of Chemistry, Binghamton University, Binghamton, New York USA 13902*

[c]*Department of Mathematics, University of Colorado Denver, Denver CO USA 80204*

***** corresponding author email: liliya.vugmeyster@ucdenver.edu

SI1. Preparation of liposome stock solution

The procedure of liposome extraction from the 12 month old hippocampus brain tissue is described in Cheng et al.[1] The tissue (kindly supplied by Dr. Terrance Deak at Binghamton University) was homogenized using a glass homogenizer with 12 strokes over a 30-second time period in 0.32 M HEPES-buffered sucrose solution (4mM HEPES, pH 7.4). The solution was then centrifuged at 900 Xg for 10 minutes at 4 ºC, and the pellet was collected and re-suspended in 0.32 M HEPES-buffered sucrose. The solution was centrifuged for the second time at 10,000 Xg for 15 minutes at 4 ºC and the pellet was collected again. The pellet was lysed in 4 mL deionized water and transferred to a glass homogenizer and then homogenized with 3 strokes. Then 16 uL of 1.0 HEPES buffer was quickly added to the above solution to reach the final HEPES concentration 4.0 mM. This diluted solution was then rotated at 4 ºC for 30 minutes for a completed lysing and was centrifuged at 25,000 Xg for 20 minutes at 4 ºC. The pellet was collected, and the synaptic plasma membranes were enriched in a discontinuous sucrose gradient containing 1.2 M, 1.0 M and 0.8 M HEPES-buffered sucrose solution layers with the volume ratio 3.5:3.0:3.0. The vesicles were collected by centrifuging the depositions with sucrose gradient solutions at 150,000 Xg for 2 hours at 4 ºC, and the sample (at the bottom of the 1.0M / 1.2 M HEPES-buffered sucrose solution interphase) was collected using an 18 G needle and a 1 mL syringe. The pellet was re-suspended finally in 4.0 mM HEPES buffer and stored at -80 ºC until use. This suspension is referred to as the liposome stock solution in the main text.

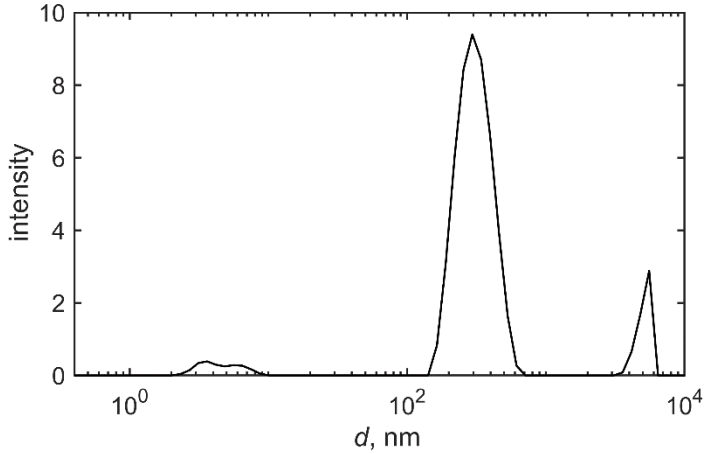

Figure S1. Dynamic light scattering intensity at the scattering angle of 90º versus particle diameter *d*, corrected for the phosphate buffer background. The data were collected using Malvern Zeta S90 instrument using 60 s correlograms averages of 5 sets, with 50 repetitions per set. The liposome suspensions used in the seeded growth protocols has been diluted by a factor of 100 for these measurements.

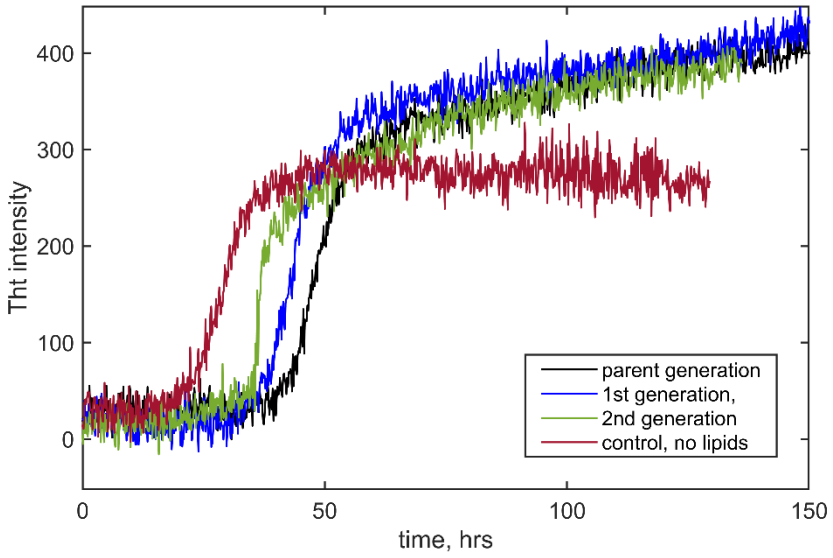

Figure S2. ThT fluorescence assays data for different generations of the seeded growth protocols described in the main text. ThT assay fluorescence intensity, in arbitrary units, as a function of time. The concentration of $A\beta_{1-40}$ was 25 μM for all generations and the molar ratio of lipids to proteins was 20:1 in the parent generation, 2:1 in the first generation, and 0.2:1 for the second generation. The data represents the average of three independent measurements for each sample and were corrected for the appropriate backgrounds, which were pure buffer for the Aβ control with no lipides, and the membrane solution in the buffer for all other samples. The measurements were performed using standard protocols[2] using BioTek Cytation3 plate reader with the excitation and emission wavelength set at 450 and 490 nm, respectively. Readings were taken at the bottom of the wells at 25°C every 10 min preceded by mixing for 20 s at 307 rpm. The ThT dye concentration was 40 μM.

SI2. Decomposition of the line shape to obtain the fraction of the bound state in the N-terminal domain residues.

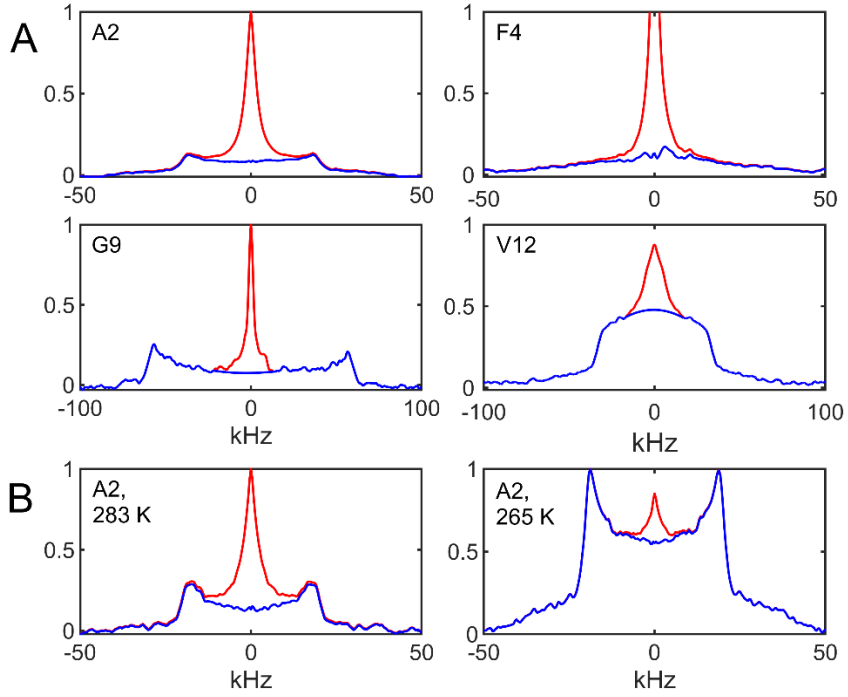

Figure S3. A) Line shape decomposition to obtain p_{bound} values for the N-terminal residues in mem A$\beta_{1\text{-}40}$ fibrils, collected in the 305-310 K temperature range. The experimental spectra for the mem fibrils are shown in red, while the obtained bound fraction is shown in blue. The procedure involves separating the non-Lorentzian component to obtain the fraction of the bound state, with the details listed in reference[3] and is summarized below. B) The spectra for additional two temperatures for the A2 residue.

At the physiological temperature, the line shapes significantly narrowed (Figure 3 of the main text), indicating the presence of large-scale motions on the relevant timescale. The narrow component is attributed to the free states undergoing motions approximated by the isotropic diffusion. The wide component is attributed to the "bound" state, which lacks diffusive motions, presumably due to interactions with the rigid fibril core.

The p_{bound} for the A2, F4, and V12 residues is quantified by decomposing the line shape into the Lorenzian and non-Lorenzian components,[3] the latter of which is attributed to the bound state. Similar to the treatment of the wild-type fibrils, the analysis for the G9 site is somewhat more complex. For the G9 residue, we have seen that a part of the non-Lorenzian component is not due to the bound state per se and the best approach is to assume that the bound state corresponds to the fraction of the rigid-like (full powder pattern) line shape in the overall shape.[3, 4] The "horns" of the rigid powder-pattern are clearly visible for G9 in the mem fibrils even at the physiological temperature.

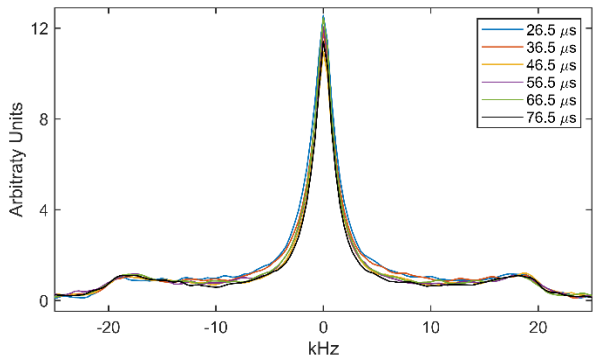

Figure S4. Experimental ^{2}H quadrupolar echo line shapes for the A2-CD_3 site in mem Aβ fibrils collected with different echo delays at 299 K, indicated directly on the panel. The line shapes are normalized to match the heights of the wide component (bound fraction), and variations in the intensity of the central peak thus indicate the variations in the resulting free fractions. Using the line shape decomposition described above, this amounts to up to 5% variations in p_{bound}.

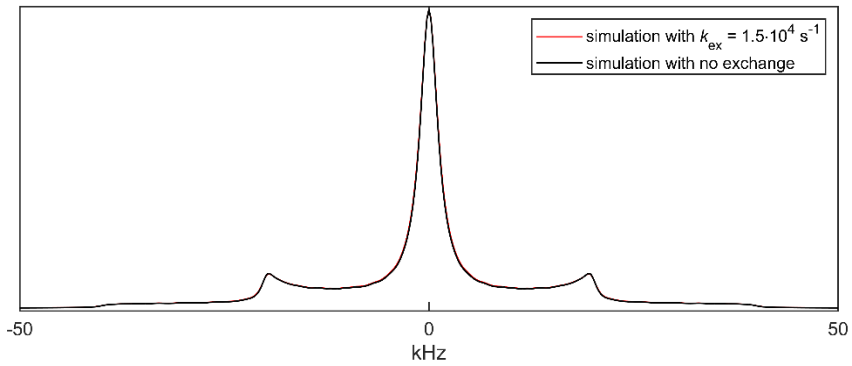

Figure S5. Simulated ^{2}H line shapes for the A2-CD_3 site in mem fibrils using the two-state model of figure 1F of the main text and calculated with (red line) or without (black line) the explicit inclusion of the conformational exchange. The simulations are performed using the following values p_{bound}=0.4, D=5.9· 10^5 rad^2/s, k_{ex} 1.5·10^4 s^{-1}, C_{q} 53.5 kHz, and echo delay of 26.5 μs. The explicit inclusion of the exchange does not affect the line shapes. The same result was obtained for different values of echo delays in the 26 to 66 μs range.

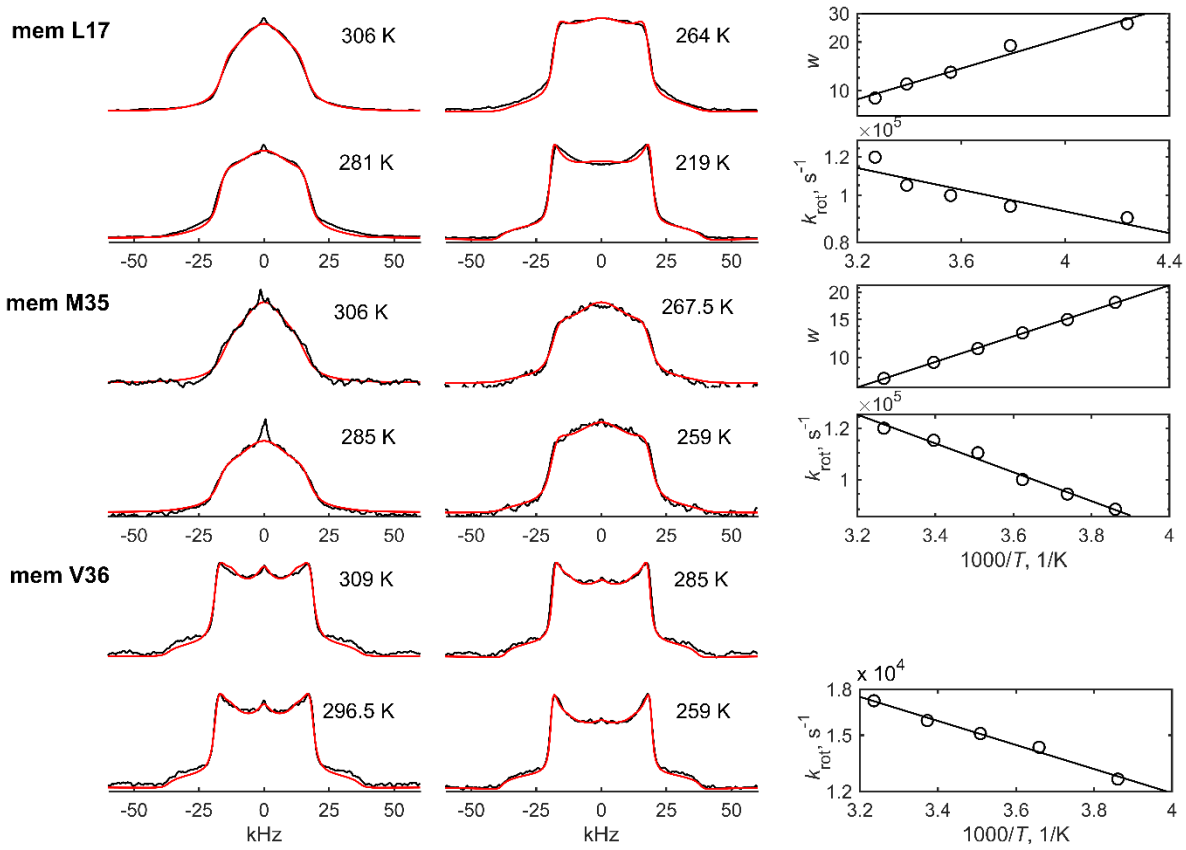

Figure S6. Experimental line shape data, collected at 9.4 T, and the corresponding line shape fits for L17, M35, and V36 methyl sites of the mem fibrils. Normalized experimental line shapes (black lines) are overlaid with simulations (red lines). The panels to the right show corresponding Arrhenius and Boltzmann-type plots for k_{rot} and w, respectively. Note that for the mem V36 site it was sufficient to use the values of w that were fixed at the values obtained for the wt fibrils to avoid ambiguities in the fitting procedure. Fitting the data for L17, L34, and M35 sites required the use of the iterative procedure as detailed in prior work. It is also interesting to note that for the M35 site the line shapes in the 250 to 200 K temperature range coincided with the ones obtained for the wt fibrils.[5] In the lower temperature range fewer conformers are populated and a different model of three rotamers rather than four was used in the fits of the wt fibrils.

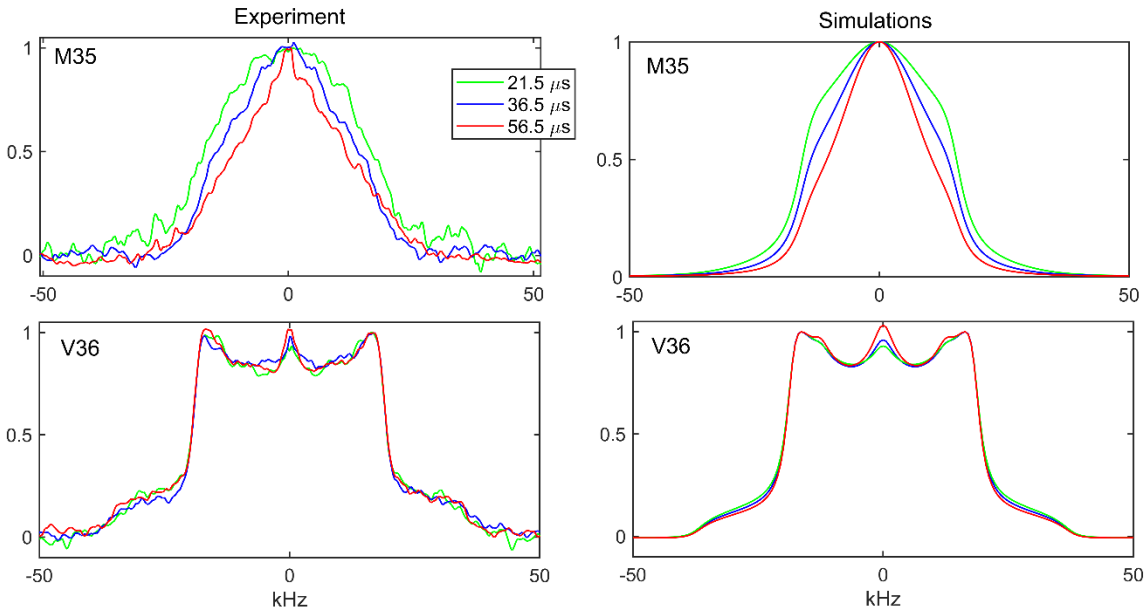

Figure S7. Experimental (left) and simulated (right) deuterium static QE line shapes for the methyl sites of M35 and V36 in the mem $A\beta_{1\text{-}40}$ fibrils recorded using different values of the quadrupolar echo delays (τ), shown directly on the panels. The temperatures were 306 K for the M35 site and 309 K for the V36 site. For the M35 site there is a qualitative agreement in the τ-dependence patterns seem in the simulations and the experiment. For the V36 site, there is little τ-dependence in the experimental spectra within the uncertainties, while the simulated one show minor modulations at the central region around the zero frequency. Note, that in the experimental spectra there are residual minor contributions of the HOD signals form water, thus these modulations observed in simulations would be difficult to discern in the background of the water signal, which itself can have τ-dependence.

SI3. Additional ^{2}H T_1 experimental data details and fitting procedures for the F19-ring-D$_5$ site

For the purpose of signal enhancement, the multiple echo acquisition scheme[6, 7] was used in the longitudinal ^{2}H T_1 measurements at the F19 ring site. In this scheme, the spectrum is broken into a series of spikelets, the distance between which in the frequency domain is encoded by the echo spacing delay in the time domain. In our case the spikelets appear every 16 kHz, and an example of the spectrum is shown in Figure S5A. The magnetization build-up curves can then be obtained at the chosen spikelets. The scheme preserves the relaxation anisotropy,[8] which in our case is rather significant. Figure S5B presents examples of magnetization build-up curves for the ±16 and ±64 kHz spikelets. We also observe, in similarity to the case of the wt fibrils,[9] that relaxation is non-exponential, reflecting the heterogeneity of core packing.[10, 11] The build-up curves are fitted by the stretch-exponential function of the form[12, 13]

$$M(t) = M(\infty)(1 - e^{-(t/T_1^{eff})^{\beta}}), \qquad \text{(Eq. S1)}$$

in which $M(t)$ is the signal intensity, T_1^{eff} is the effective relaxation time, and β is the parameter that reflects the degree of non-exponentiality, defined in the range of $0 < \beta \leq 1$.[11, 13] β less than 1 corresponds to non-exponential behavior. The presence of a significant non-exponentiality, well in excess of what might be expected from a simple orientational dependence, is an indicator of the distribution of the ring-flip constants.

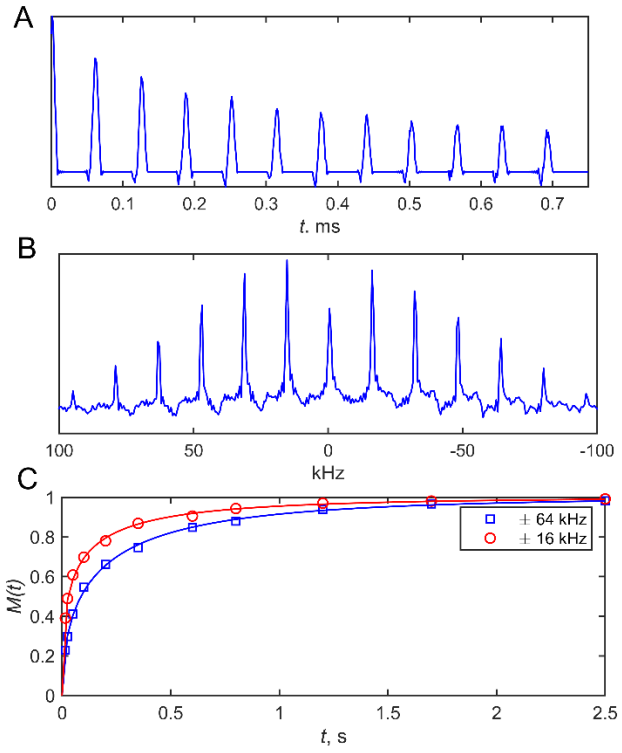

Figure S8. An example of raw data for the ^{2}H T_1 relaxation times saturation recovery measurements performed for the mem fibrils, deuterated at the ring of the F19 residue. The data shown were collected 303 K and 9.4 T under static conditions. A) An example of FID collected with a multiple echo acquisition scheme and the pulse spacing of 63 μs. B) The corresponding spectrum, obtained with the 0.2 kHz line broadening function, demonstrating the spikelets separated by the 16 kHz intervals. C) Normalized magnetization build-up curves for the sum of intensities of the spikelets at the ±16 kHz (red) and ±64 kHz positions (blue). The lines represent the fits to the stretched-exponential function of Eq. S1.

The values of T_1^{eff} and β for all temperatures (shown in Figure S6) are fitted to the global model of Figure 1F of the main text, [9, 14] which assumes the energy landscape with a gaussian distribution of activation energies for the ring-flipping motions. The main fitting parameters are $\langle E_a^{flip} \rangle$,the central value, and σ^{flip}, the width of distribution, assuming that each individual rate constants within the ensemble follows the Arrhenius temperature dependence.

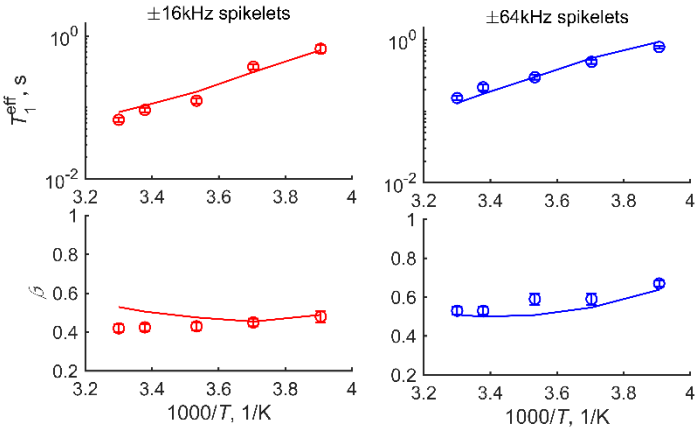

Figure S9. ^{2}H static solid state NMR longitudinal relaxation data for mem fibrils at the F19-ring-D_5 site at 9.4 T, collected with the multiple echo acquisition scheme. The values of T_1^{eff} and β versus 1000/T, obtained for the two sets of spikelet positions, indicated directly on the panels, resulting from the fits of the magnetization build-up curves to the stretched exponential function of Eq. S1. The lines represent the fits to the global model that allow for determination of the ring-flipping activation energies distribution.

The parameters of the small-angle fluctuations around the χ_2 angle (Figure 1F) were fixed at the values determined for the 2-fold wt fibrils:[9] $\langle E_a^{small} \rangle$ =10.5 kJ/mol, σ^{small}= 1.7 kJ/mol, and the single Arrhenius prefactor of 2.17 ·10^{10} s^{-1}. The quadrupolar tensor parameters were C_q=180 kHz, η=0. The angles between either the C^{δ}–D or the C^{ε}–D bonds and the C^{β} – C^{γ} axis was taken as 59.2°. The amplitude of the small-angle fluctuations in the 4-site jump model of Figure 2D was taken as $\alpha/2$ = 5°. The errors in the fitted model parameters were determined using the inverse covariance matrix method.

References

1. Q. Cheng, Z. W. Hu, Y. Tobin-Miyaji, A. E. Perkins, T. Deak and W. Qiang, *Biomolecules*, 2020, **10**.
2. L. P. Jameson, N. W. Smith and S. V. Dzyuba, *ACS Chem. Neurosci.*, 2012, **3**, 807-819.
3. D. F. Au, D. Ostrovsky, R. Fu and L. Vugmeyster, *J. Biol. Chem.*, 2019, **294**, 5840–5853.
4. L. Vugmeyster, D. F. Au, D. Ostrovsky, B. Kierl, R. Fu, Z. W. Hu and W. Qiang, *Biophys. J.*, 2019, **117**, 1524-1535.
5. L. Vugmeyster, M. A. Clark, B. I. Falconer, D. Ostrovsky, D. Gantz, W. Qiang and G. L. Hoatson, *J. Biol. Chem.*, 2016, **291**, 18484-18495.
6. F. H. Larsen, H. J. Jakobsen, P. D. Ellis and N. C. Nielsen, *Chem. Phys. Lett.*, 1998, **292**, 467-473.
7. F. H. Larsen, H. J. Jakobsen, P. D. Ellis and N. C. Nielsen, *J. Phys. Chem. A*, 1997, **101**, 8597-8606.
8. R. L. Vold, G. L. Hoatson, L. Vugmeyster, D. Ostrovsky and P. J. De Castro, *Phys. Chem. Chem. Phys.*, 2009, **11**, 7008-7012.

9. L. Vugmeyster, D. Ostrovsky, G. L. Hoatson, W. Qiang and B. I. Falconer, *J. Phys. Chem. B*, 2017, **121**, 7267–7275.
10. W. Schnauss, F. Fujara, K. Hartmann and H. Sillescu, *Chem.Phys. Lett.*, 1990, **166**, 381-384.
11. L. Vugmeyster, D. Ostrovsky, K. Penland, G. L. Hoatson and R. L. Vold, *J. Phys. Chem. B*, 2013, **117**, 1051-1061.
12. P. A. Beckmann and E. Schneider, *J. Chem. Phys.*, 2012, **136**, 054508.
13. H. Sillescu, *J. NonCryst. Sol.*, 1999, **243**, 81-108.
14. L. Vugmeyster, D. Osrovsky, T. R. Villafranca, J. Sharp, W. Xu, A. S. Lipton, G. L. Hoatson and R. L. Vold, *J. Phys. Chem. B.*, 2015, **119**, 14892–14904.